FLUORESCENCE REDISTRIBUTION AFTER PHOTOBLEACHING

A New Multipoint Analysis of Membrane Translational Dynamics

Dennis E. Koppel, *Department of Biochemistry, University of Connecticut Health Center, Farmington, Connecticut 06032 U.S.A.*

ABSTRACT A theoretical formulation and experimental methodology are presented for a new multipoint analysis of membrane translational dynamics. The redistribution of fluorescent probe after a localized photobleaching pulse is monitored at several locations by a focused laser beam sequentially scanned through the bleached area. The spatial information so obtained provides a unique sensitivity to possible systematic flow and a direct internal calibration of the characteristic transport distance. These capabilities are demonstrated with experimental data on a reconstituted multibilayer system.

INTRODUCTION

The past few years have seen a surge of interest in the fluid dynamics of cell plasma membranes and its function as an indicator and possible effector of physiological changes (1–4). Many physical approaches have been applied in this area, most notably a variety of magnetic resonance and fluorescence techniques. Among these, the recently developed technique of "fluorescence photobleaching recovery" has proved especially useful for the measurement of lateral diffusion in membranes over macroscopic distances (5–9). In this technique (also referred to as "fluorescence recovery after photobleaching"), translational transport in the plane of the membrane is characterized by the kinetics of fluorescence "recovery," due to the spatial redistribution of fluorescently labeled molecules, after an initial, localized, irreversible photobleaching pulse. In this way, diffusion coefficients have been determined for phospholipids, glycolipids, and proteins both in reconstituted bilayer membranes and cell plasma membranes (e.g., 8–23).

With a single noteworthy exception (5), all fluorescence photobleaching experiments have used a laser light source. Typically, the same laser beam, focused to a small, circularly symmetric spot on the sample, has been used as a bleaching beam and, when appropriately attenuated by a neutral density filter, as a monitoring beam. (An interesting alternative approach has recently been described (21–23) in which photobleaching is used to form a periodic pattern of fluorescence, taking direct advantage of the extreme simplicity of the Fourier transform of the diffusion equation.) A characteristic recovery time is determined from a single trace of fluorescence excited by the monitoring beam at the bleaching position. The size ($1/e^2$ radius of an assumed Gaussian profile) of the focused laser beam spot, needed

for the calculation of absolute transport parameters, is determined by various means in separate experiments.

Data of this type suffer from two basic limitations: insensitivity to the direction and speed of possible systematic flow processes, and a limited ability to separate them from random diffusion; and large uncertainty in the characteristic transport distance. The first of these restricts the investigation of possible directed membrane flow in cell systems (e.g., reference 24). It can also lead to an overestimation of a diffusion coefficient if an artifactual drift goes unrecognized. In the absence of flow, the uncertainty of beam size is the largest source of absolute error.

In the multipoint analysis introduced below, the fluorescence redistribution after photobleaching is monitored by a focused laser beam sequentially positioned at each of several locations in and adjacent to the bleached area. As we shall see, the additional spatial information thus obtained provides both a sensitivity to systematic flow and a direct means of distance calibration.

THEORY

In this section, theoretical expressions are derived for the fluorescence intensity as a function of position and time after a photobleaching pulse. We make the following basic assumptions: (*a*) Preceding the photobleaching pulse, the fluorescently labeled molecules are in effect uniformly distributed on an infinite plane. The prebleach fluorescence intensity is thus independent of the position of the monitoring laser beam, and is designated $F(-)$. (*b*) $c(\underset{\sim}{r},t)$, the concentration of fluorescent molecules at position $\underset{\sim}{r}$ at time t after a photobleaching pulse centered at $\underset{\sim}{r} = 0$, changes due to the redistribution of molecules in the plane of the membrane. There is no chemical recovery. The molecular motion is characterized by diffusion coefficient D and systematic flow velocity $\underset{\sim}{v}$. The presence of an immobile component (i.e., one with $D = 0$) can be incorporated in obvious ways.

Define $F(\underset{\sim}{\Delta}r, t)$ as the fluorescence intensity at time t excited by a monitoring beam centered at a position shifted $\underset{\sim}{\Delta}r$ relative to the bleaching beam. Then

$$F(\underset{\sim}{\Delta}r, t) = q \int I(\underset{\sim}{r} - \underset{\sim}{\Delta}r)c(\underset{\sim}{r}, t)\mathrm{d}^2\underset{\sim}{r}, \tag{1}$$

where $I(\underset{\sim}{r} - \underset{\sim}{\Delta}r)$ is the spatial profile of the monitoring beam at $\underset{\sim}{\Delta}r$, and q is the product of all the quantum efficiencies of light absorption, emission, and detection. $c(\underset{\sim}{r}, t)$, defined above, can be related to $c(\underset{\sim}{r}, 0)$, the concentration profile immediately after the bleaching pulse, by the following relation (25):

$$c(\underset{\sim}{r}, t) = \int G(\underset{\sim}{r} - \underset{\sim}{r}', t)c(\underset{\sim}{r}', 0)\mathrm{d}^2\underset{\sim}{r}', \tag{2}$$

where $G(\underset{\sim}{r} - \underset{\sim}{r}', t)$ is the probability per unit area that a molecule at point $\underset{\sim}{r}'$ at time 0 will be at point $\underset{\sim}{r}$ at the time t. For the type of motion under consideration,

$$G(\underset{\sim}{r}'', t) = (4\pi Dt)^{-1} \exp(-|\underset{\sim}{r}'' - \underset{\sim}{v}t|^2/4Dt). \tag{3}$$

Combining Eqs. 1 and 2, and substituting $\underset{\sim}{r}'' \equiv \underset{\sim}{r} - \underset{\sim}{r}'$, we have

$$F(\underset{\sim}{\Delta}r,t) = q \int I(\underset{\sim}{r} - \underset{\sim}{\Delta}r) \int G(\underset{\sim}{r}'', t)c(\underset{\sim}{r} - \underset{\sim}{r}'', 0)\mathrm{d}^2\underset{\sim}{r}''\mathrm{d}^2\underset{\sim}{r}. \tag{4}$$

In previous analyses (7), the fluorescence intensity, considered only at $\underset{\sim}{\Delta}r = 0$, was evaluated for specific functional forms of $I(\underset{\sim}{r})$ and $c(\underset{\sim}{r} - \underset{\sim}{r}'', 0)$. It was assumed that both the bleaching and monitoring beams had the same uniform or Gaussian profile, and that the fluorophore bleached with first-order kinetics. With the additional spatial information available to us now, however, it is no longer necessary to make explicit assumptions about beam profiles or bleaching kinetics. Instead, $F(\underset{\sim}{\Delta}r, t)$ can be simply related to $F(\underset{\sim}{\Delta}r, 0)$, a measurable function. Changing the order of integration in Eq. 4, we have

$$F(\underset{\sim}{\Delta}r, t) = q \int G(\underset{\sim}{r}'', t) \int I(\underset{\sim}{r} - \underset{\sim}{\Delta}r)c(\underset{\sim}{r} - \underset{\sim}{r}'', 0)\mathrm{d}^2\underset{\sim}{r}\mathrm{d}^2\underset{\sim}{r}''. \tag{5}$$

The integral over $\underset{\sim}{r}$ can now be evaluated with the aid of Eq. 1, giving

$$F(\underset{\sim}{\Delta}r, t) = \int G(\underset{\sim}{r}'', t)F(\underset{\sim}{\Delta}r - \underset{\sim}{r}'', 0)\mathrm{d}^2\underset{\sim}{r}''. \tag{6}$$

Analytical expressions for $F(\underset{\sim}{\Delta}r, t)$ can be derived for assumed forms of $F(\underset{\sim}{\Delta}r - \underset{\sim}{r}'', 0)$. We consider two different geometries: 1. The bleaching and monitoring beams are focused (or defocused) by a cylindrical lens to produce a "line" very much longer than it is wide. This geometry has practical advantages, discussed below, if one is limited to a one-dimensional beam scan (see Discussion). 2. The beam profiles are the usual circularly symmetric "spots" in the $x-y$ plane.

In both cases, we assume that the fluorescence scans are Gaussian, i.e.,

$$F_1(\underset{\sim}{\Delta}r - \underset{\sim}{r}'', 0)/F(-) = 1 - \alpha_0 \exp\{-[\hat{x} \cdot (\underset{\sim}{\Delta}r - \underset{\sim}{r}'')]^2/w_0^2\}, \tag{7}$$

and

$$F_2(\underset{\sim}{\Delta}r - \underset{\sim}{r}'', 0)/F(-) = 1 - \alpha_0 \exp(-|\underset{\sim}{\Delta}r - \underset{\sim}{r}''|^2/w_0^2). \tag{8}$$

In these equations, the subscripts 1 and 2 refer to the line and spot geometries defined above, α_0 is a constant ($0 < \alpha_0 < 1$) that characterizes the extent of bleaching, and $\hat{x}$ is a unit vector along the x-axis, perpendicular to the orientation of the line. w_0 is the $1/e$ radius of the assumed Gaussian fluorescence scan, equivalent to an effective laser beam size. As we shall see, actual measured fluorescence scan profiles follow this Gaussian form to a remarkable extent. Combining Eqs. 3 and 6–8, integrating over $\underset{\sim}{r}''$, we have finally:

$$F_1(\underset{\sim}{\Delta}r, t)/F(-) = 1 - \alpha_1(t) \exp\{-[\hat{x} \cdot (\underset{\sim}{\Delta}r - \underset{\sim}{v}t)]^2/w^2(t)\} \tag{9}$$

and

$$F_2(\underset{\sim}{\Delta}r, t)/F(-) = 1 - \alpha_2(t) \exp[-|\underset{\sim}{\Delta}r - \underset{\sim}{v}t|^2/w^2(t)], \tag{10}$$

with

$$w^2(t) = w_0^2(1 + t/\tau_D), \tag{11}$$

$$\alpha_1(t) = \alpha_0/(1 + t/\tau_D)^{1/2}, \tag{12}$$

$$\alpha_2(t) = \alpha_0/(1 + t/\tau_D), \tag{13}$$

where

$$\tau_D = w_0^2/4D \tag{14}$$

is the charcteristic time for diffusion.

It is interesting to note that if the fluorescence scan is Gaussian at time zero, it remains Gaussian for all times thereafter. As a result, Eqs. 9–14 apply for a time "zero" corresponding to any postbleach time. This property can be put to practical use in the analysis of data as a means of avoiding possibly difficult extrapolations. It is also clear at this point how $\underset{\sim}{v}$, τ_D, w_0, and hence D, can be calculated from the time-course of the central position, amplitude, and width of $F(\underset{\sim}{\Delta}r, t)$, determined in a single experiment.

METHODS

Fig. 1 shows a schematic diagram of the optical apparatus designed to perform the multipoint analysis. It shares many features in common with a standard photobleaching optical system. The laser beam (Control Laser Corporation, Orlando, Fla.; model 554 A/K mixed gas ion laser) is attenuated to an appropriate degree (neutral density filter, ND), and directed by mirrors (M) into the back of the incident-light fluorescence illuminator of a Leitz Ortholux II microscope (E. Leitz, Inc., Rockleigh, N.J.). Lens L1 is an auxiliary microscope objective that adjusts the final focus of the laser beam at the sample. A cylindrical lens is added before L1 for line-bleach experiments. A dichroic mirror (DM) reflects the laser beam down through the microscope objective L2 (which thus acts as both the condensor and light collector) but allows the sample fluorescence to be transmitted up to the photomultiplier tube (PMT), located in a thermoelectrically cooled housing supported above the microscope. DM is thus in a

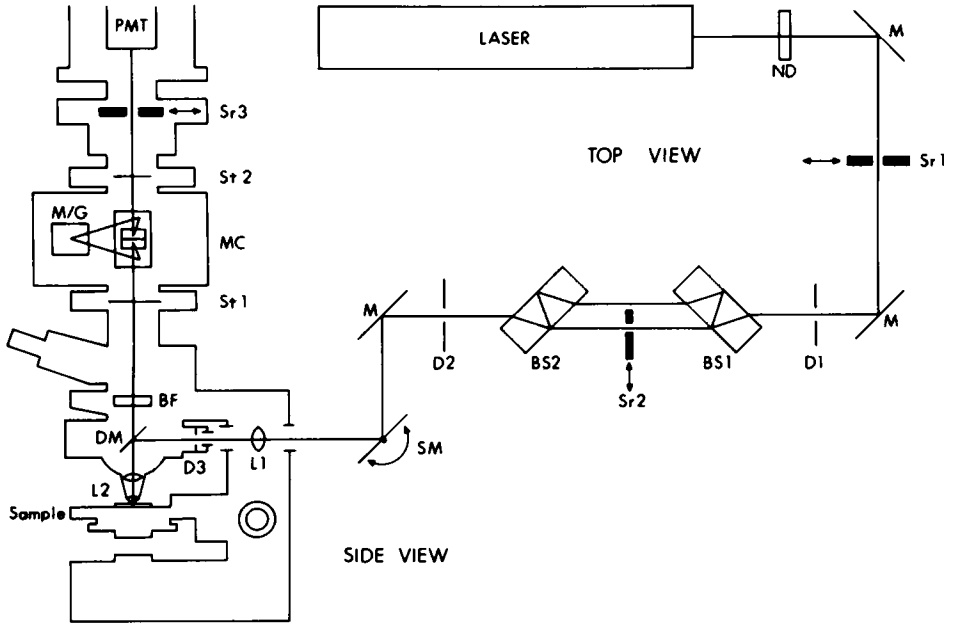

FIGURE 1 Schematic diagram of the optical apparatus. The symbols used are: ND, neutral density filter; Sr, shutter; M, mirror; D, diaphragm; BS, beam splitter; SM, scanner mirror; L, lens; DM, dichroic mirror; BF, barrier filter; St, slit; MC, monochrometer housing; M/G, mirror or grating; PMT, photomultiplier tube.

position to act also as a barrier filter along with BF to block the back-scattered and reflected excitation light. The PMT is protected from the high level of fluorescence emitted during the bleaching pulse by an electronic shutter Sr3. The whole of the optical system is mounted on an optical table, isolated from floor vibrations by pneumatic pistons.

The system incorporates several unique features that improve the performance and increase the power and flexibility of the basic technique. The combination of diaphragms D1 and D2, uncoated beamsplitters BS1 and BS2, and electronic shutter Sr2 work together to switch the laser intensity between bleaching levels and monitoring levels. With Sr2 open, a nearly unattenuated beam, transmitted through BS1 and BS2 without reflection, passes through diaphragm D2. This provides the bleaching beam. With Sr2 closed, however, only that beam reflected four times, once at each glass-to-air interface, is in a position to pass through D2. This attenuates the beam by a factor of $\sim 10^4$ ($\sim$ 10% is reflected each time), producing the monitoring beam. This system has several advantages over previous approaches in which a bleaching beam is produced with the removal of a neutral density filter. It is fast. (Sr2 is a standard shutter that can be opened and closed in a little more than 1 ms.) The monitoring beam is undistorted and alignment between the bleaching and monitoring beams is guaranteed. (The surfaces of BS1 and BS2 are flat to within $\lambda/10$ and parallel to within 2 s of arc.)

The precise orientation of the incident laser beam, and hence the location on the sample of the focused beam along a scan axis, is modulated by a servo-activated galvanometric optical scanning mirror (SM, General Scanning, Inc., Watertown, Mass.; model G-100PDT). SM can position the beam on the sample with an accuracy and reproducibility of better than 0.1 μm. Less than 1 ms is needed for a full-scale deflection. The microscope is equipped with a rotating object stage so that the sample can be properly oriented relative to the scanning axis.

A real image of the fluorescent sample is formed in the plane of the entrance slit (St1) of a monochrometer housing (MC). The resulting spatial discrimination acts to block the major part of background fluorescence excited above or below the in-focus object plane (6). In normal operation, component M/G is a mirror (M) that reflects all the fluorescence through the exit slit St2. When desired, however, the mirror can be replaced with the regular monochrometer grating (G) for the measurement of fluorescence emission spectra.

The PMT signal is processed by special photon-counting electronics. After pulse amplification-discrimination-shaping, the detected fluorescence signal consists of a series of standardized pulses, each corresponding to the detection of a single photon. These pulses are then counted within contiguous intervals timed by a crystal oscillator clock. 1,024 consecutive sums, each representing the experimental estimate of the fluorescence intensity at a given time, are stored in a 12 K-bit random access memory. The data are converted to analog form for a continuous scope display and for a hard-copy plot. The beam-scanner, bleaching shutters, data recording, and read-out are timed and synchronized by special digital electronics.

There are two major data-taking modes. In one, the focused laser beam is sequentially positioned at up to twelve discrete locations on the membrane, each of which can be specified independently with a bank of thumbwheel digital switches. Bleaching can be effected at any or all of the positions. In the other, an adjustable delay can be inserted between high-resolution sequential scans. Data taken under these conditions, with or without an initial bleaching pulse, can give repetitive "pictures" of a cell surface as it evolves over a long period of time.

Δx, the distance from the center of the focused laser beam along the scan axis, is simply related to $\Delta\theta$, the angular deflection of the scanning mirror. To a good approximation,

$$\Delta x = 2f\Delta\theta, \tag{15}$$

where f is the effective focal length of the microscope objective combined with L1 and the optics of the incident illuminator. The gain of the optical scanner can be adjusted and calibrated relative to a stage micrometer. Fig. 2 presents data of the intensity of laser light reflected from a stage micrometer, detected with barrier filter BF removed, in a scan adjusted to a nominal gain of 10 μm/24 points. Data points are circled at 24-point intervals for purposes of evaluation. These data, as well as that of the following section, were taken with a laser wavelength of 4,765 Å, using a $\times$10, 0.25 NA objective.

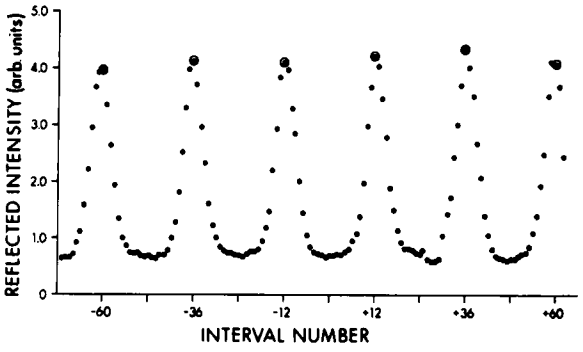

FIGURE 2 Intensity of laser light reflected from stage micrometer (10 μm smallest division) with nominal scan gain of 10 μm/24 intervals. Data is circled at 24-point intervals. A ×10, 0.25 NA achromat was employed, with an incident wavelength of 4,765 Å.

RESULTS

The data presented in this section were selected to demonstrate the features and capabilities of the multipoint analysis. For purposes of comparison, all measurements were performed on a single sample—a reconstituted planar multibilayer membrane composed of a 1:1.3:1 mixture by weight of phospholipids, matrix protein, and lipopolysaccharide, isolated from the outer membrane of gram negative bacteria *Escherichia coli* and *Salmonella typhimurium*. Before reconstitution, the fluorescent probe N-4-nitrobenzo-2-oxa-1,3-diazole phosphotidylethanolamine (NBD-PE) was added to the phospholipid mixture at a molar ratio of 1:1,000. The preparation and characterization of such membranes are described in detail elsewhere.[1]

Fig. 3 presents a set of recovery curves of NBD-PE fluorescence measured with a circularly symmetric laser spot sequentially positioned at 12 equally spaced locations separated by 1.0 μm. The bleaching pulse was centered at the seventh location. The top graph, for simplicity, shows fluorescence data from only three locations: coincident with the bleaching pulse, i.e., $\Delta x = 0$ (▲), and at $\Delta x = \pm 5.0$ μm (+, x). Note that the recovery curves on either side of center are identical, consistant with an isotropic diffusive transport mechanism. The data were fit to the following form:

$$F(\Delta x, t) = F(-)\{1 - \beta\alpha_2(t) \exp[-(\Delta x)^2/w^2(t)] - (1 - \beta)\alpha_0 \exp[-(\Delta x)^2/w_0^2]\}, \quad (16)$$

where $\beta(<1)$ represents the size of the mobile fraction. A five point fitting procedure was employed. From estimates of $F(-)$, $F(0, 0)$, $F(0, t_1)$, and $F(0, t_2)$, with t_1 and t_2 chosen so that $t_1 \simeq \tau_D$ and $t_2 \gg \tau_D$, one can analytically solve for α_0, β, and τ_D. From $F(-)$, $F(0, 0)$, and $F(\pm 5.0$ μm, 0) one can analytically solve for w_0, and hence D. The solid curves in Fig. 3 were computed according to Eqs. 11, 13, 14, and 16, with $\beta = 0.95$, $\tau_D = 10.7$ s, $w_0 = 4.49$ μm, and thus $D = 4.71 \times 10^{-9}$ cm^2/s. A $\beta < 1$, in this case, is most likely the result of imperfect membrane fusion. The bottom graph in Fig. 3 shows fluorescence data recorded at all 12 locations plotted on a 4x expanded time axis. The solid theoretical curves now trace out the

[1] Schindler, M., M. J. Osborn, and D. E. Koppel. Manuscript in preparation.

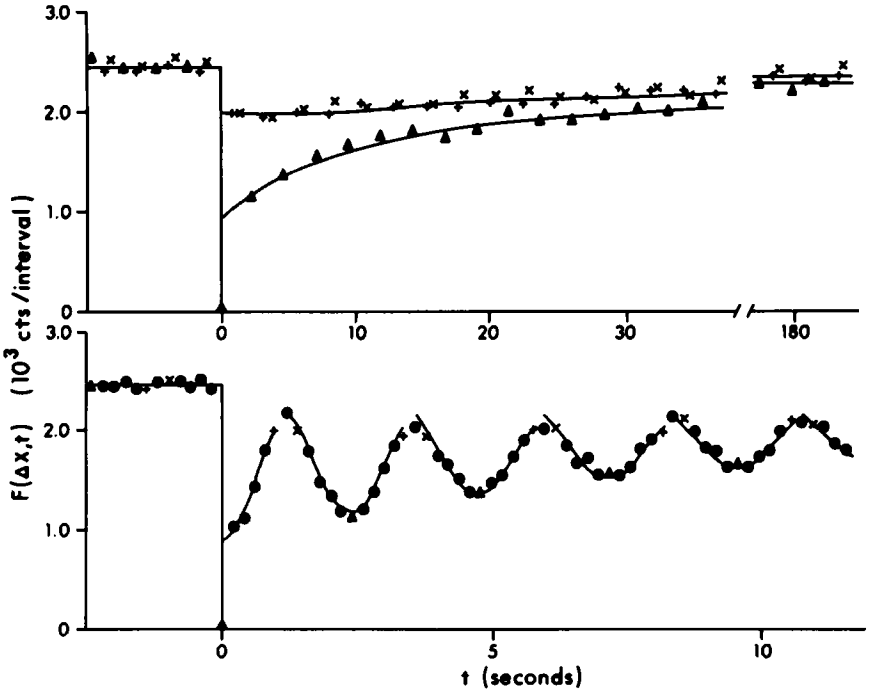

FIGURE 3 Fluorescence redistribution after photobleaching data of NBD-PE in a reconstituted multibilayer membrane (1:1.3:1 by weight phospholipid to matrix protein to lipopolysaccharide), monitored at 12 equally spaced spots (1.0 μm separation) about a single point bleach. The solid curves are a fit to theory with $\beta = 0.95$, $w_0 = 4.49$ μm, $\tau_D = 10.7$ s, $D = 4.71 \times 10^{-9}$ cm^2/s. (*top*) Recoveries measured at 3 of the 12 locations: coincident with the bleach pulse (▲), and 5.0 μm on either side of center (+, ×). (*bottom*) Sequential scans including all 12 locations on expanded time scale.

individual scans through the bleached region. The excellent agreement between the theory and data observed here justifies our original assumption of Gaussian scan profiles.

An example of data recorded on the same sample with a line bleach oriented perpendicular to the scan axis is presented in Fig. 4. As in Fig. 3, the top graph traces the recovery at 3 of 12 equally spaced locations: coincident with the bleaching pulse, and 4.0 μm on either side of center. The bottom graph shows successive 12-point fluorescence scans on an expanded time axis. The data were fit to the form of Eq. 16 with $\alpha_1(t)$ substituted for $\alpha_2(t)$. A best-fit was obtained with β and D constrained to those values determined for the data of Fig. 3, leaving $F(-)$, α_0 and w_0 as the only floating parameters. The agreement between the resulting theoretical values (the solid curves) and the data demonstrates the internal consistancy of the analysis.

Fig. 5, for completeness, presents a set of line-bleach fluorescence curves in which recovery is dominated by systematic flow along the scan axis. For this case, the entire membrane sample was moved at a velocity of 3.33 μm/s on a motorized, micrometer-driven, translational object stage. The photobleaching pulse was positioned at the first of 12 equally separated locations. The top graph shows the fluorescence intensity monitored at four locations as the bleached region is swept past. The bottom graph shows the successive 12-point scans on the

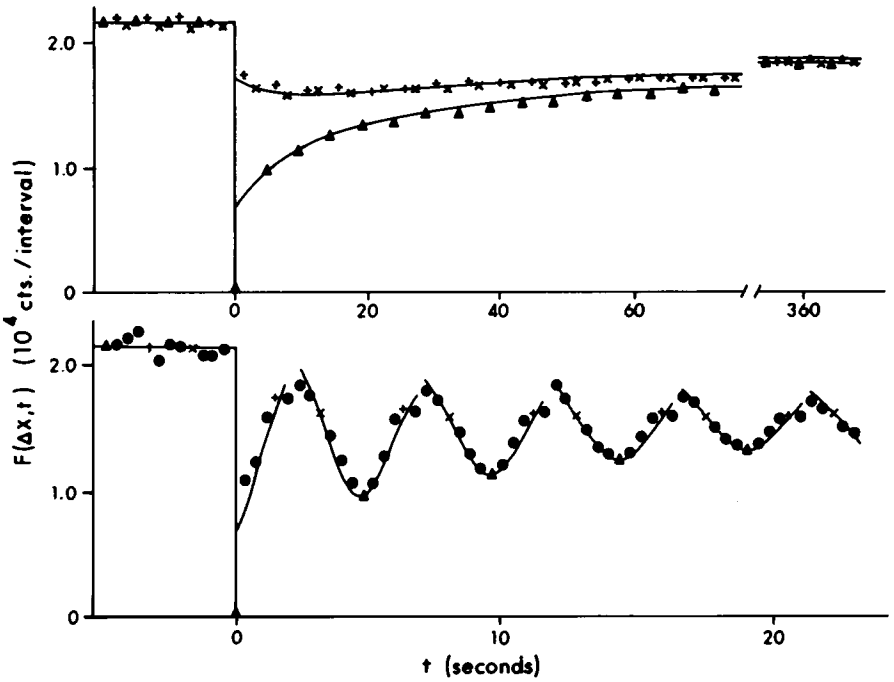

FIGURE 4 Data from the same membrane as in Fig. 3, monitored at 12 equally spaced locations (1.0 μm separation) about a single line bleach. The solid curves are a fit to theory, corresponding to $w_0 = 3.61$ μm, with β and D constrained to 0.95 and 4.71 $\times$ 10^{-9} cm^2/s, respectively. (*top*) Recoveries measured at 3 of the 12 locations: coincident with the bleaching pulse (▲), and 4.0 μm on either side of center (+, $\times$). (*bottom*) Sequential scans including all 12 locations on expanded time scale.

same time axis. Note the rapid shifting of the fluorescence minimum relative to the scan locations. Some recovery due to translational diffusion can also be observed. The theoretical curves shown were computed incorporating the known values of v, D, and β, with $F(-)$, α_0, and w_0 as the only floating parameters.

DISCUSSION

The multipoint scanning capability described above was developed primarily as a means of providing an increased sensitivity to possible systematic flow. In experiments performed with a stationary monitoring beam, a component of flow is detectable only in relatively subtle variations in the functional form of the fluorescence recovery. In the multipoint analysis, however, a component of flow velocity along the scan axis appears as a phase shift—a widening separation between the position of the fluorescence minimum and the position of the bleaching pulse. This is evident in the data of Fig. 5, an extreme case in which recovery is dominated by flow (i.e., $vw_0/4D \simeq 10$). Even when diffusion is dominant, it is still possible to recognize and quantitate a flow component along the scan axis. Systematic motion perpendicular to the scan axis would not produce such a shift, but would affect the recovery observed at each location in point bleach experiments. This latter complication is eliminated in the line geometry. The recovery curves are not affected by motion of any kind along the line axis,

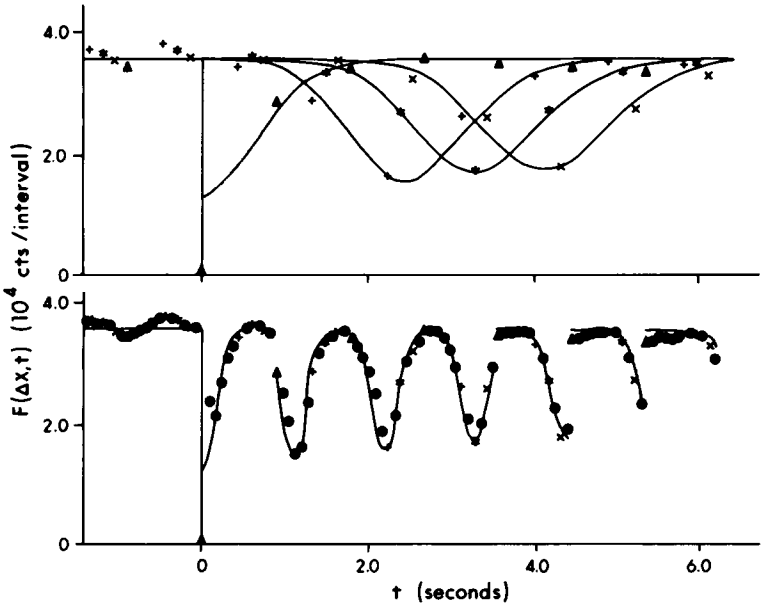

FIGURE 5 Data from the same membrane as in Figs. 3 and 4, monitored at 12 equally spaced locations (1.8 μm separation) in the line bleach geometry, as the sample was translated at a speed of 3.33 μm/s on a motorized micrometer-driven object stage. The solid curves are a fit to theory, corresponding to w_0 = 3.16 μm, with β. D, and V constrained to 0.95, 4.71 × 10^{-9} cm^2/s, and 33.3 μm/s, respectively. (top) Fluorescence measured at 4 of the 12 locations: coincident with the bleaching pulse (▲), and at 3 locations downstream (+, *, ×). (*bottom*) Sequential scans including all 12 locations.

perpendicular to the scan axis, so that systematic flow appears only as an observable phase shift. The line configuration also increases the total fluorescence signal, and opens the way for the investigation of possible anisotropic diffusion characteristics (22).

To evaluate data measured with a stationary monitoring beam, it is necessary to perform separate experiments to calibrate the beam size. This leads to problems of reproducibility. Slight variations in focus, for example, can produce relatively large changes in beam size. In the multipoint analysis, however, such variations are automatically taken into account for each set of data by the internal calibration of w_0.

Periodic pattern photobleaching (21) offers similar capabilities. A directed flow can be detected in the fluorescence images relative to some fixed reference point. The characteristic distance of transport is just the period of the photobleached pattern. The relative merits of the two approaches are determined mainly by technical considerations. The multipoint technique offers the convenience of a real-time scanning analysis. Periodic pattern fluorescence images must be individually scanned for subsequent analysis. The spatial information available with the periodic pattern approach is far more extensive, but is obtained only with a sacrifice of time resolution and detection sensitivity.

The derivations of specific analytical expressions for $F(\underset{\sim}{\Delta}r, t)$ in the multipoint analysis were based on the assumption of Gaussian scan profiles. Data have consistantly confirmed this to be a good approximation. There is every reason to believe, moreover, that even if significant deviations from a Gaussian profile do exist, the transport parameters extracted from the data

will still be reliable. It has been shown empirically that calibrating the beam size with separate photobleaching scan experiments will automatically compensate for wide variations of the functional forms of $I(r)$ and $c(r, 0)$ in the calculated values of D (Eq. 22, reference 7). The same will apply to the values of D calculated with the internal scan calibration of w_0. Values of v calculated from phase-shifts along the scan axis are totally independent of scan profile. The analysis presented here can thus provide the basis for a rigorous quantitation of translational dynamics.

This investigaton was supported by research grant GM23585 from the U.S. Public Health Services, and a grant from the University of Connecticut Research Foundation.

Received for publication 8 June 1979 and in revised form 30 July 1979.

REFERENCES

1. EDIDIN, M. 1974. Rotational and translational diffusion in membranes. *Annu. Rev. Biophys. Bioeng.* **3**:179–201.
2. EDELMAN, G. M. 1976. Surface modulation in cell recognition and cell growth. *Science (Wash. D.C.).* **192**:218–226.
3. NICOLSON, G. L. 1976. Transmembrane control of the receptors on normal and tumor cells. *Biochim. Biophys. Acta.* **457**:57–108.
4. SHINITZKY, M., and M. INBAR. 1976. Microviscosity parameters and protein mobility in biological membranes. *Biochim. Biophys. Acta.* **433**:133–149.
5. PETERS, R., J. PETERS, K. H. TEWS, and W. BAHR. 1974. A microfluorometric study of translational diffusion in erythrocyte membranes. *Biochim. Biophys. Acta.* **367**:282–294.
6. KOPPEL, D. E., D. AXELROD, J. SCHLESSINGER, E. L. ELSON, and W. W. WEBB. 1976. Dynamics of fluorescence marker concentration as a probe of mobility. *Biophys J.* **16**:1315–1329.
7. AXELROD, D., D. E. KOPPEL, J. SCHLESSINGER, E. ELSON, and W. W. WEBB. 1976. Mobility measurements by analysis of fluorescence photobleaching recovery kinetics. *Biophys. J.* **16**:1055–1069.
8. EDIDIN, M., Y. ZAGYANSKY, and T. J. LARDNER. 1976. Measurements of membrane protein lateral diffusion in single cells. *Science (Wash. D.C.).* **191**:466–468.
9. JACOBSON, K., E-S. WU, and G. POSTE. 1976. Measurement of the translational motion of concanavalin A in glycerol-saline solutions and on the cell surface by fluorescence recovery after photobleaching. *Biochim. Biophys. Acta.* **433**:215–222.
10. SCHLESSINGER, J., D. E. KOPPEL, D. AXELROD, K. JACOBSON, W. W. WEBB, and E. L. ELSON. 1976. Lateral mobility on cell membranes: Mobility of concanavalin A receptors on myoblasts. *Proc. Natl. Acad. Sci. U.S.A.* **73**:2409–2413.
11. JACOBSON, K., Z. DERZKO, E-S. WU, Y. HOU, and G. POSTE. 1976. Measurement of the lateral mobility of cell surface components in single living cells by fluorescence recovery after photobleaching. *J. Supramol. Struct.* **5**:565–576.
12. AXELROD, D., P. RAVDIN, D. E. KOPPEL, J. SCHLESSINGER, W. W. WEBB, E. L. ELSON, and T. R. PODLESKI. 1976. Lateral motion of fluorescently labeled acetylcholine receptors in membranes of developing muscle fibers. *Proc. Natl. Acad. Sci. U.S.A.* **73**:4594–4597.
13. SCHLESSINGER J., D. AXELROD, D. E. KOPPEL, W. W. WEBB, and E. L. ELSON. 1977. Lateral transport of a lipid probe and labeled proteins on a cell membrane. *Science (Wash. D.C.)* **195**:307–310.
14. WOLF, D. E., J. SCHLESSINGER, E. L. ELSON, W. W. WEBB, R. BLUMENTHAL, and P. HENKART. 1977. Diffusion and patching of macromolecules on planar lipid bilayer membranes. *Biochemistry.* **16**:3476–3483.
15. WU, E-S., K. JACOBSON, and D. PAPAHADJOPOULOS. 1977. Lateral diffusion in phospholipid multibilayers measured by flourescence recovery after photobleaching. *Biochemistry.* **16**:3936–3941.
16. SCHLESSINGER, J., E. L. ELSON, W. W. WEBB, I. YAHARA, U. RUTISHAUSER, and G. M. EDELMAN. 1977. Receptor diffusion on cell surfaces modulated by locally bound concanavalin A. *Proc. Natl. Acad. Sci. U.S.A.* **74**:1110–1114.
17. AXELROD, D., P.M. RAVDIN, and T. R. PODLESKI. 1978. Control of acetylcholine receptor mobility and distribution in cultured muscle membranes - a fluorescence study. *Biochim. Biophys. Acta.* **511**:23–38.

18. WU, E-S., K. JACOBSON, F. SZOKA, and A. PORTIS. 1978. Lateral diffusion of a hydrophobic peptide, N-4-nitrobenz-2-oxa-1,3 diazole gramicidin S in phospholipid multibilayers. *Biochemistry.* **17**:5543–5550.
19. FAHEY, P. F., and W. W. WEBB. 1978. Lateral diffusion in phospholipid bilayer membranes and multilamellar liquid crystals. *Biochemistry.* **17**:3046–3053.
20. JOHNSON, M., and M. EDIDIN. 1978. Lateral diffusion in plasma membrane of mouse egg is restricted after fertilization. *Nature (Lond.).* **272**:448–450.
21. SMITH, B. A., and H. M. MCCONNELL. 1978. Determination of molecular motion in membranes using periodic pattern photobleaching. *Proc. Natl. Acad. Sci. U.S.A.* **75**:2759–2763.
22. SMITH, B. A., W. R. CLARK, and H. M. MCCONNELL. 1979. Anisotropic molecular motion on cell surfaces. *Proc. Natl. Acad. Sci. U.S.A.* In press.
23. SMITH, L. M., J. W. PARCE, B. A. SMITH, and H. M. MCCONNELL. 1979. Antibodies bound to lipid haptens in model membranes diffuse as rapidly as the lipids themselves. *Proc. Natl. Acad. Sci. U.S.A.* In press.
24. BRETSCHER, M. S. 1976. Directed lipid flow in cell membranes. *Nature (Lond.).* **260**:21–23.
25. CRANK, J. 1956. The Mathematics of Diffusion. Oxford University Press, London. 26–27.